Cerebral Cortex, September 2017;27: 4423–4435

doi: 10.1093/cercor/bhw244
Advance Access Publication Date: 1 September 2016
Original Article

ORIGINAL ARTICLE

Dopamine D2 Receptors Enhance Population Dynamics in Primate Prefrontal Working Memory Circuits

Torben Ott and Andreas Nieder

Animal Physiology, Institute of Neurobiology, Auf der Morgenstelle 28, University of Tübingen, 72076 Tübingen, Germany

Address correspondence to Email: andreas.nieder@uni-tuebingen.de

Abstract

Working memory is associated with persistent activity in the prefrontal cortex (PFC). The neuromodulator dopamine, which is released by midbrain neurons projecting into the frontal lobe, influences PFC neurons and networks via the dopamine D1 (D1R) and the D2 receptor (D2R) families. Although behavioral, clinical and computational evidence suggest an involvement of D2Rs in working memory, a neuronal explanation is missing. We report an enhancement of persistent working memory responses of PFC neurons after iontophoretically stimulating D2Rs in monkeys memorizing the number of items in a display. D2R activation improved working memory representation at the population level and increased population dynamics during the transition from visual to mnemonic representations. Computational modeling suggests that D2Rs act by modulating interneuron-to-pyramidal signaling. By increasing the population's response dynamics, D2Rs might put PFC networks in a more flexible state and enhance the neurons' working memory coding, thereby controlling dynamic cognitive control.

Key words: dopamine, dopamine D2 receptor, macaque monkey, prefrontal cortex, working memory

Introduction

The persistent activation of prefrontal cortex (PFC) neurons in the absence of external stimulation is considered a neuronal correlate of working memory, which is the ability to briefly retain and manipulate information in mind (Fuster 2008). During working memory, stimuli are processed flexibly from moment to moment depending on the behavioral context and current goals mediating cognitive control (Baddeley 2012). Working memory, and executive control functions in general, are influenced by midbrain dopamine neurons that project to PFC. There, dopamine affects PFC neurons via the dopamine D1 receptor (D1R) and D2 receptor (D2R) families (Robbins and Arnsten 2009).

While D1Rs have been shown to modulate working memory and other executive functions on both behavioral (Sawaguchi and Goldman-Rakic 1991; Müller et al. 1998; Noudoost and Moore 2011; Puig and Miller 2012) and neuronal level (Williams and Goldman-Rakic 1995; Vijayraghavan et al. 2007; Puig and Miller 2012; Ott et al. 2014), the role of D2Rs has been less clear. Behaviorally, D2Rs stimulation can improve working memory performance in primates (Mehta et al. 2001; Gibbs and D'Esposito 2005; Von Huben et al. 2006) and D2Rs are involved in cognitive flexibility and attention (Floresco and Magyar 2006; Noudoost and Moore 2011; Stelzel et al. 2013; Puig and Miller 2015). Clinical evidence suggests a prominent role of D2Rs in psychiatric diseases characterized by disturbed executive control and psychosis (Winterer and Weinberger 2004; Rolls et al. 2008). Supported by computational modeling studies, D2Rs were hypothesized to increase cognitive flexibility by putting PFC working memory networks in a flexible state (Durstewitz and Seamans 2008; Rolls et al. 2008) enabling dynamic cognitive control (Stokes et al. 2013; Cools 2015).

Despite this evidence, a neuronal correlate of D2R influence on working memory signals is lacking. In a previous single-cell study in monkeys required to memorize the location of saccade targets, D2R manipulation had a strong impact on eye movement-related discharges, but no effect on the preceding persistent spatial working memory signal (Wang et al. 2004). So far, the underlying physiological basis for D2Rs modulation of working memory is still unknown.

We hypothesized that D2Rs modulate persistent working memory activity in PFC neurons. Therefore, we trained two macaque monkeys to remember visual items that represented different numerosities, thus involving feature-based working memory processing as opposed to spatial working memory (Nieder 2002; Viswanathan and Nieder 2013; Jacob and Nieder 2014; Nieder 2016). By combining single unit recordings with iontophoretic drug application and computational modeling, we show that D2R stimulation indeed increases working memory coding at the single neuron level and enhances the response dynamics of prefrontal neuronal populations.

Materials and Methods

Animals and Surgical Procedures

Two male rhesus monkeys (*Macaca mulatta*) were implanted with a titanium head post and one recording chamber centered over the principal sulcus of the lateral PFC, anterior to the frontal eye fields (right hemispheres in both monkeys). Surgery was conducted using aseptic techniques under general anesthesia. Structural magnetic resonance imaging was performed before implantation to locate anatomical landmarks and reconstruct recording sites with stereotactic coordinate (Fig. 1D). All experimental procedures were in accordance with the guidelines for animal experimentation approved by the authority, the Regierungpsräsidium Tübingen, Germany.

Task

Monkeys performed a memory-guided decision-making task, comparing sample numerosities (set sizes) with test numerosities. They initiated a trial by grasping a lever and maintaining central fixation on a screen. After a pure fixation period (500 ms), a sample stimulus (500 ms) cued the animals for the reference numerosity (i.e., number of dots) they had to remember in the subsequent memory delay period (delay 1, 1000 ms) without numerosities. The first memory interval was followed by a rule-cue (300 ms) that instructed the monkeys to select either a larger number of dots ("greater than" rule) or a smaller number of dots ("less than" rule) than the sample numerosity in the subsequent test phase. The test phase was preceded by a second delay (delay 2, 1000 ms) requiring the monkeys to assess the rule at hand for the subsequent choice. In the following test 1 phase, the monkeys had to release the lever in a "greater than" trial, if the number of items in the test display was larger than the number of items in the sample display, or to keep holding the lever for another 1200 ms until the appearance of a second test display (test 2), if the number of items in the test display was smaller than the number of items in the sample display. In a "less than" trial, these conditions were reversed. Monkeys got a liquid reward for a correct choice. Thus, only test 1 required a decision; test 2 was used so that a behavioral response was required in each trial, ensuring that the monkeys were paying attention during all trials. Because both sample and test numerosities varied randomly, the monkeys could only solve the task by assessing the numerosity of the test display relative to the three possible numerosities of the sample display together with the appropriate rule in any single trial. To test a range of numerosities, both monkeys were presented with numerosities 2 (smaller test numerosity = 1, larger test numerosity = 4), 8 (4:16), and 32 (16:64). For any sample numerosity, test numerosities were either larger or smaller with equal probability ($p = 0.5$). Because the monkeys' numerosity discrimination performance obeys the Weber–Fechner law (Nieder and Miller 2003), numerosities larger than the sample numerosity need to be numerically more distant than

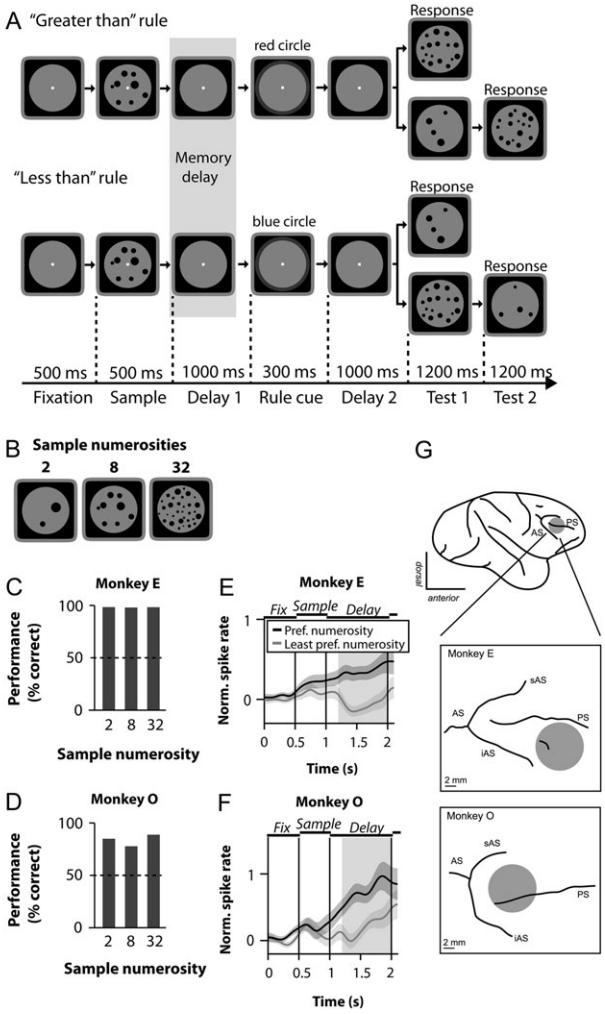

Figure 1. Memory-guided decision-making task and behavioral performance. (*A*) Memory-guided decision-making task. Monkeys grabbed a bar and fixated a central fixation spot throughout the trial. They had to remember a sample numerosity (number of dots) during the memory delay period (delay 1). After presentation of a rule cue indicating either the "greater than"- (red circle) or "less than"-rule (blue circle), the monkeys were required to respond (by releasing the bar) to test-displays showing more or fewer dots, respectively, than the sample numerosity to receive a reward. (*B*) Example sample stimuli. For each session, new random dot patterns were created, using different patterns for all sample-test combinations. (*C*) Behavioral performance (% correct) for monkey E for the range of sample numerosities ("2", "8", and "32"). (*D*) Behavioral performance of monkey O. (*E*) Population response of neurons selective for the sample numerosity of monkey E during the memory delay period. Black line, preferred numerosity, gray line, nonpreferred numerosity. Shaded areas represent SEMs across neurons. (*F*) Same conventions as in (*E*) for monkey O. (*G*) Recording site located in the right lateral PFC around the principal sulcus for both monkeys (red shaded area). AS = arcuate sulcus, iAS = inferior limb of AS, sAS = superior limb of AS, PS = principal sulcus.

numerosities smaller than the sample numerosity to reach equal discriminability. Based on this design, any test numerosity (except the smallest and largest used) served as test numerosities for different sample numerosities, thus preventing the animals from learning systematic relations between numerosities.

To prevent the animals from exploiting low-level visual cues (e.g., dot density, total dot area), a standard numerosity protocol (with dot sizes and positions pseudo-randomized) and a control numerosity protocol (with equal total area and average density of all dots within a trial) were each presented in 50% of the trials in a pseudo-randomized fashion. Each rule was signified by two different rule-cues in two different sensory modalities: a red circle ("greater than" rule, red color) or a white circle with a drop of water ("greater than" rule, water) signified the rule "greater than". The "less than" rule was cued by a blue circle ("less than" rule, blue color) or a white circle with no water ("less than" rule, no-water). We showed in previous studies that monkeys generalize the numerical principles "greater than" and "less than" to numerosities they had never seen before (Eiselt and Nieder 2013). Before each session, the displays were generated anew using MATLAB (Mathworks). Trials were randomized and balanced across all relevant features (sample numerosities, "greater than" and "less than" rules, rule-cue modalities, standard and control stimuli, match and non-match trials). Monkeys had to keep their gaze within 1.75° of the fixation point from the fixation interval up to the onset of the first test stimulus (monitored with an infrared eye-tracking system; ISCAN, Burlington, MA).

Electrophysiology and Iontophoresis

Extracellular single-unit recording and iontophoretic drug application was performed as described previously (Jacob et al. 2013; Ott et al. 2014). In each recording session, up to three custom-made tungsten-in-glass electrodes flanked by two pipettes each were inserted transdurally using a modified electrical microdrive (NAN Instruments). Single neurons were recorded at random; no attempt was made to preselect the neurons to any task-related activity or based on drug effects. Signal acquisition, amplification, filtering, and digitalization were accomplished with the MAP system (Plexon). Waveform separation was performed offline (Offline Sorter; Plexon). Drugs were applied iontophoretically (MVCS iontophoresis system; npi electronic) using custom-made tungsten-in-glass electrodes flanked by two pipettes each (Thiele et al. 2006; Jacob et al. 2013; Ott et al. 2014). Electrode impedance and pipette resistance were measured after each recording session. Electrode impedances were 0.8–3 MΩ (measured at 500 Hz; Omega Tip Z; World Precision Instruments). Pipette resistances depended on the pipette opening diameter, drug, and solvent used. Typical resistances were 15–50 MΩ (full range, 12–160 MΩ). As in previous experiments (Jacob et al. 2013; Ott et al. 2014), we used retention currents of –7 nA to hold the drugs in the pipette during control conditions. The ejection current for SKF81297 (10 mM in double-distilled water, pH 4.0 with HCl; Sigma-Aldrich) was +15 nA, the ejection current for SCH23390 (10 mM in double-distilled water, pH 4.0 with HCl; Sigma-Aldrich) was +25 nA, and the ejection current for quinpirole (10 mM in double-distilled water, pH 4.0 with HCl; Sigma-Aldrich) was +40 nA. In control experiments with 0.9% physiological NaCl, pH 4.0 with HCl, the ejection current was +25 nA. We did not investigate dosage effects and chose ejection currents to match the values reported to be maximally effective, i.e., in the peak range of the "inverted-U" (Wang et al. 2004; Vijayraghavan et al. 2007). In these studies, D1R agonists have been shown to be most effective at moderate doses of 15 nA (Vijayraghavan et al. 2007). For D1R antagonists, 25 nA has been repeatedly used and shown to yield specific effects (Williams and Goldman-Rakic 1995; Vijayraghavan et al. 2007). For D2R agonists, which have not been shown to modulate delay period activity previously, larger doses have yielded stronger effects on saccade-related activity (Wang et al. 2004). Thus, we used 40 nA to try maximizing potential D2R effects. For each recording session, one pipette per electrode was filled with drug solution (either SKF81297, SCH23390, quinpirole or NaCl), and the other always contained 0.9% NaCl. We used the same drug for all pipettes within the same recording session. The drugs used are highly selective for D1Rs (SKF81297, SCH23390) or D2Rs (quinpirole) and show very little affinities for the corresponding other receptor family (Seeman and Van Tol 1994). In addition, they are highly specific and show only little affinity to other receptors such as serotonin receptors (Hyttel 1983; Andersen and Jansen 1990, Levant et al. 1992). In each recording session, control conditions using the retention current alternated with drug conditions using the ejection current. Drugs were applied continuously for 12–15 min (drug conditions), depending on the number of trials completed correctly by the animal. Each control or drug application block consisted of 72 correct trials to yield sufficient trials for analysis. The first block (12–15 min) was always the control condition. Given that iontophoretic drug application is fast and can quickly modulate neuronal firing properties (Jacob et al. 2013), we did not exclude data at the current switching points.

Data Analysis

Selection Criteria

All well-isolated recorded single units with a baseline spike rate above 0.5 Hz (determined in the 500 ms fixation period preceding sample presentation) and with at least 15 trials for each of the three sample numerosities in each control and drug condition entered all subsequent analyses. Neurons were not included based on drug effects. Only correct trials were analyzed.

Numerosity-Selective Neurons

We calculated a two-way ANOVA for each neuron to determine if a neuron's response was correlated with sample numerosities in the memory delay period (delay 1), thus representing a numerosity in working memory. We used spike rates in an 800 ms window beginning 200 ms after sample offset, based on previous studies (Bongard and Nieder 2010; Vallentin et al. 2012). The main factors were numerosity ("2"/"8"/"32") and iontophoresis condition (control conditions/drug conditions). We identified numerosity-selective neurons by a significant main factor of the factor numerosity ($p < 0.05$). Since the monkeys' behavior did not show any differences for standard and control stimuli, and because we have shown previously that neuronal responses in the PFC do not differentiate between standard and control stimuli (Bongard and Nieder 2010), we pooled over standard and control stimuli trials.

Single-cell and Population Responses

For plotting single-cell spike density histograms, the average firing rate in trials with one of the three different sample numerosities (correct trials only) was smoothed with a Gaussian kernel (bin width of 200 ms, step of 1 ms). Tuning

curves were constructed by calculating mean spike rates in the same analysis window used for the ANOVA. For the population responses, we defined a neuron's preferred numerosity as the numerosity yielding the higher average spike rate in the analysis window used for the ANOVA, averaging over control and drug trials. Accordingly, the intermediate and least preferred numerosities were defined as the numerosities resulting in lower average spike rates. Neuronal activity was normalized by subtracting the mean baseline firing rate in the control condition and dividing by the standard deviation of the baseline firing rates in the control condition. For population histograms, normalized activity was averaged and smoothed with a Gaussian kernel (bin width of 200 ms, step of 1 ms). Population tuning curves were calculated as the mean normalized activity for each condition in the same analysis windows used for the ANOVA.

Neuronal Information About Sample Numerosities

We estimated the information a single unit carried about the sample numerosity during working memory by using three different quantifications. Calculations were performed based on spike rates in the delay period using the same analysis window as for the ANOVA. Additionally, we performed sliding window analysis, using spike rates in overlapping 100 ms windows stepped in 10 ms increments from fixation onset to the end of the delay 1 period. First, we defined a tuning index (TI) by subtracting the neuron's spike rate to the least preferred sample numerosity from the spike rate of the preferred numerosity and dividing by the sum, i.e.,

$$TI = \left(FR_{pref} - FR_{leastpref}\right)/\left(FR_{pref} + FR_{leastpref}\right).$$

TIs vary between 0 and 1, expressing the relative (rather than absolute) differences in spike rates between sample numerosities, where low values correspond to low numerosity selectivity and high values correspond to high numerosity selectivity. Second, we calculated the percentage explained variance (PEV) using ω^2, expressing how much of a neuron's spike rates can be explained by the sample numerosity (Jacob and Nieder 2014). ω^2 is defined as

$$\omega^2 = \left(SS_{groups} - df \times MSE\right)/(SS_{total} + MSE),$$

where the individual terms are calculated using a one-way ANOVA using all three sample numerosities as levels (pooled over control and drug condition). SS_{groups} is the sum of squares between groups (sample numerosities), SS_{total} the total sum of squares, df the degree of freedoms, and MSE the mean squared error. The number of trials in each group was balanced by stratifying the number of trials in each group to the minimum trial number across groups, randomly selecting individual trials. This process was repeated 25 times, and the mean of the stratified values was taken as the final statistic. ω^2 is an unbiased, zero-mean statistic when there is no information, while values above zero indicates the variance explained by the sample numerosity (Jacob and Nieder 2014). Values range roughly from 0 to 1, expressing the fraction of explained variance in the data explained by the task variable (i.e. ω^2 values of 0.1–0.2 correspond to 10–20% "percent" explained variance). Third, sample numerosity coding quality was quantified using receiver operating characteristic (ROC) analysis derived from Signal Detection Theory. The area under the ROC curve (AUROC) is a nonparametric measure of the discriminability of two distributions. It denotes the probability with which an ideal observer can tell apart a meaningful signal from a noisy background. Values of 0.5 indicate no separation, and values of 1 signal perfect discriminability. The AUROC takes into account both the difference between distribution means as well as their widths and is therefore a suitable indicator of signal quality. We used AUROCs to quantify the quality of sample numerosity coding in the memory period. We calculated the AUROC for each neuron using the spike rate distributions of the preferred and the least preferred numerosity in the same analysis window used for the ANOVA.

Linear Regression Analysis

We used linear regression analysis to estimate the neuronal population coding of numerosities in working memory, disentangling general drug-induced neuronal activity changes and variability of neuronal responses explained by numerosity. Analysis was performed following Mante et al. (2013) and is described in detail in Supplementary Materials. In brief, neuronal data was binned (100 ms, 50 ms steps) and z-scored. We then estimated regression coefficients for numerosity for each neuron and time bin, describing how much of the trial-by-trial variability of a neuron depends on the sample numerosity. Regression coefficients were averaged during the delay 1 period, yielding a time independent estimate of each neuron's numerosity coding strength during working memory. To quantify the population's momentary numerosity evidence, we projected the population response onto the population vector containing the regression coefficients. All analyses steps and control analyses (shuffled data, cross-validation and simulations) are described in Supplementary Materials.

Principal Component Analysis

We performed principal component analysis (PCA) to represent the population activity of all recorded single units in a low-dimensional subspace, extracting shared activity patterns prominent in the population response (Cunningham and Yu 2014). Analysis is described in detail in the Supplementary Materials. In brief, neuronal data was binned (100 ms, 50 ms steps), z-scored and trial-averaged. By considering the activity of all neurons in each time bin and condition as pseudo-simultaneous, we performed PCA to represent neuronal population activity using the first three principal components capturing the largest amount of variance in population response, accounting for 42% (for quinpirole data) of the total variance. The distance between pair-wise trajectories in state space was calculated as the Euclidean distance using the full *n*-dimensional space. Trajectory velocity was calculated as the Euclidean distance between two adjacent time bins divided by the time step (Stokes et al. 2013). Distance and velocity was baseline-normalized using condition-specific baselines in control and drug conditions. All analyses steps and control analyses (shuffled data, cross-validation and simulations) are described in the Supplementary Materials.

Neural Network Model

We implemented a neural network model to investigate possible synaptic mechanisms by which D2Rs modulate delay period activity. Network architecture and parameters were identical to Brunel and Wang (2001) and are described in detail in Supplementary Materials. In brief, the model consisted of pyramidal cells and interneurons described by leaky integrate-and-fire neurons. Excitatory connections from pyramidal cells to pyramidal cells and from pyramidal cells to interneurons

consisted of AMPA and NMDA currents. Inhibitory connections from interneurons to interneurons and from interneurons to pyramidal cells were modeled as GABA currents. The network shows two distinct stable attractor states (Brunel and Wang 2001; Wang 2002): Without stimulation, pyramidal cells in the network show a low-firing spontaneous activity state dominated by GABA currents (Brunel and Wang 2001). When transiently stimulating a subset of pyramidal cells with strong recurrent excitatory connections, the neurons' activity switch to a high-firing persistent activity state dominated by NMDA currents. We implemented neuromodulation by systematically changing synaptic conductances within the model and investigating effects on the network's attractor states. Model implementation was realized using Python and the brian simulator (Goodman and Brette 2009). Model architecture, equations and parameters are described in Supplementary Materials.

Results

We trained monkeys to memorize the number of items over a brief delay period ('memory delay' in Fig. 1A) in a delayed response task (Bongard and Nieder 2010; Ott et al. 2014). The monkeys had to assess the number of dots shown on a sample display, and maintain this sample numerosity in working memory during the delay period. Next, a rule cue was presented that instructed the monkeys to respond to a subsequent test display showing either more or less dots than the sample display. Thus, the delay phase after sample presentation constituted a pure working memory period (devoid of motor preparation) which allowed for investigation of neuronal working memory processes.

While the monkeys performed this task with varying numerosities and rules proficiently (Fig. 1B–D), we recorded 310 randomly selected single neurons from the lateral PFC of two macaque monkeys (Fig. 1G). For monkey E, recording locations of 206 neurons comprised areas in dorso-lateral PFC (area 9/46d and 9/46 v). For monkey O, recording was performed from 104 neurons in ventro-lateral PFC (areas 9/46 v, 47/12 and 45 A) (Petrides 2005). To directly assess the impact of dopamine receptor targeting agents on neuronal working memory activity, each neuron was recorded both without drug application (*control condition*) and while stimulating dopamine receptor agents at the vicinity of the recorded neurons using microiontophoresis (*drug condition*) (Thiele et al. 2006; Jacob et al. 2013). Control conditions alternated with drug conditions in each recording session in blocks of about 12 min. In each session we tested one of three different substances that selectively targeted the D2R or the D1R: The D2R was assessed in 76 neurons (55 monkey E, 21 monkey O) by applying the D2R agonist quinpirole. The D1R was tested in 82 neurons (25 monkey E, 57 monkey E) using the D1R agonist SKF81297, and in 85 neurons (59 monkey E, 26 monkey O) using the D1R antagonist SCH23390. To verify drug-specific effects, 67 neurons were recorded using normal saline (monkey E). In general, D2R stimulation slightly increased the neuron's spiking activity, while D1R stimulation slightly decreased neuronal activity (Ott et al. 2014).

We identified single units selectively encoding the sample numerosities during the memory delay (delay 1; see Fig. 1A) using a 2-way-ANOVA with main factors sample numerosity ("2", "8", "32") and drug condition (control, pharmacological application). Many neurons were tuned to one of the presented numerosities in the delay period (Nieder 2002; Jacob and Nieder 2014). For monkey E, 24 out of 206 (13%) recorded neurons were numerosity-selective. For monkey O, the percentage of numerosity-selective neurons was similar (13 our of 104 neurons; 13%) and not different from monkey E ($p = 0.85$, Fisher's exact test). The population activity of numerosity-selective neurons showed a similar profile, with increasing differentiation in neuronal activity between the neuron's preferred and nonpreferred numerosities (Fig. 1E,F). We combined neuronal data of both monkeys in the following analyses except where noted.

A representative delay-selective unit (Fig. 2A) showed characteristic tuning for one of the sample numerosities, i.e. a higher discharge rate for their preferred numerosity ("2" in this neuron) and increasingly lower discharge rates for more distant numerosities. After D2R stimulation with quinpirole, response differences of the same neuron to different memorized numerosities were increased, enhancing neuronal selectivity and tuning curve (Fig. 2B). To analyze averaged responses and tuning curves of the entire population of selective neurons, we ordered each neuron's delay-selective discharges to the three presented numerosities by its respective preferred, intermediate preferred and least preferred numerosity. A comparison of the population averaged spike rates in the control (Fig. 2C) and drug conditions (Fig. 2D), showed enhanced differentiation of the responses to the three memorized numerosities during D2R stimulation, and a steepening of the population averaged tuning curves (Fig. 2D).

D2R Stimulation Enhanced Working Memory Coding at the Single Neuron Level

To quantify the neuronal delay selectivity across time, we defined a sliding tuning index (TI) (Fig. 3A) (see *Materials and Methods*). The TI was significantly enhanced by D2R stimulation for delay-selective neurons (Fig. 3B) (TI = +0.11 mean ± 0.04 SEM, $p = 0.01$, signed rank test). As a measure of effect size, we derived the percentage of explained variance (PEV, expressed as absolute values ω^2, ranging roughly from 0 to 1 fraction of explained variance) by the variable "numerosity" across time for all selective neurons, calculated using a sliding ANOVA (Fig. 3C) (see *Materials and Methods*). The PEV also increased after D2R stimulation (Fig. 3D) (ΔPEV = +0.06 ± 0.02, $p = 0.01$, signed rank test). To quantify coding quality, we compared discharge rates of the neuron's preferred and least preferred sample numerosity by calculating the area under the receiver operating characteristic (AUROC) across time (Fig. 3E). D2R stimulation significantly increased AUROCs in the delay period (ΔAUROC = +0.11 ± 0.03, $p = 0.003$, signed rank test), indicating an enhancement of the neurons' working memory coding quality (Fig. 3F). This enhancement was observed for all comparisons between the most, intermediate and least preferred numerosity (Fig. S1). The modulation of numerosity was similar in both monkeys. For the 8 selective neurons recorded from monkey E (out of a total of 12 neurons from both monkeys) the ΔAUROC was +0.08 (± 0.03), and for the 4 selective neurons from monkey O the ΔAUROC was +0.17 (± 0.07). In addition, we analyzed D2R-induced changes of working memory coding by including all recorded neurons (delay-selective or not, $n = 76$) and observed the same increase in coding strengths and comparable results when analyzing data of individual monkeys (monkey E, $n = 55$; monkey O, $n = 21$) (Fig. S2). The effect of pharmacological manipulation was confirmed through application of saline (NaCl) which did not result in any coding changes (Fig. S5A–H). Thus, D2R stimulation improves memory-delay selectivity for quantities at the single neuron level.

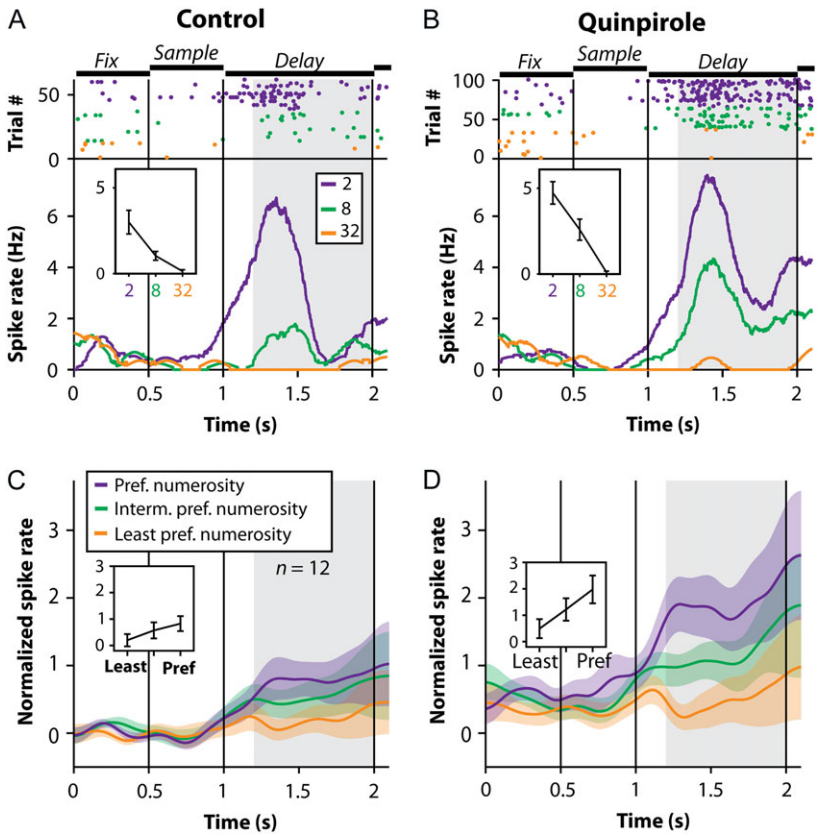

Figure 2. D2R modulation of working memory-selective neurons. (*A*) Dot-raster histogram (*top*; each dot represents an action potential; colors indicate the three numerosities) and spike-density histograms (*bottom*) of an example neuron. The neuron was tuned to numerosity "2", with lower activity for more distant numerosities (inset tuning curve in delay 1 period). (*B*) After D2R stimulation, the same neuron as in (*A*) showed enhanced and more selective tuning (layout as in (*A*)). (*C*) Time course of average normalized response of all numerosity-selective delay neurons; trials grouped according to the neurons' preferred numerosity (inset tuning curve in delay 1 period). (*D*) Same neurons as in (*C*), after D2R stimulation. Population responses were enhanced and tuning was steeper (layout as in (*C*)).

D2R Stimulation Enhanced Working Memory Coding at the Population Level

To describe numerosity representation at the population level, we used linear regression disentangling general drug-induced shifts of neuronal activity from neuronal activity explained by numerosity (Mante et al. 2013). By modeling interactions between drug and sample numerosity, we defined numerosity-related axes for control and drug conditions and projected the population response of all 76 neurons tested with the D2R-agonist onto these axes. This provided an estimate of the numerosity representation during working memory at the population level for control and drug conditions (see Materials and Methods).

Relative to the control condition (Fig. 4A), D2R stimulation prominently increased numerosity representation by the neuronal population during the entire delay period (Fig. 4B). We quantified the selectivity between numerosities responses by calculating the distance between state trajectories (in Fig. 4A,B) for all sample combinations. Compared to control conditions (Fig. 4C), stimulation of D2Rs enhanced discrimination between numerosities in the delay period (Fig. 4D). Average trajectory differences increased after D2R stimulation (Fig. 4E) (change in mean Δtrajectory = +1.1 ± 0.19, $p = 0.001$, bootstrapping). Moreover, the regression weights for the task variable 'numerosity' were increased by D2R stimulation, as witnessed by a positive interaction term (Fig. 4F, mean interaction term = +0.021 ± 0.006, $p = 0.003$, signed rank test). D2R stimulation enhanced working memory coding in neuronal population of both monkeys independently. For monkey E, the average trajectory differences increased after D2R application (Fig. 4G) (change in mean Δtrajectory = +0.87 ± 0.18, $p = 0.01$, bootstrapping). Likewise, the average trajectory difference was enhanced after D2R application for monkey O, too (Fig. 4H) (change in mean Δtrajectory = +1.29 ± 0.34, $p = 0.03$, bootstrapping). We confirmed the results of the regression analysis by using shuffled data and cross-validation (Fig. S6). To confirm that overall drug-induced shifts in spiking activity cannot explain the results, we simulated data applying the same strength of numerosity coding and the same amount of drug-induced shifts in overall spiking activity (Fig. S6). These controls verified that general changes in neuronal activity did not drive specific D2R modulation of working memory. Application of saline (NaCl) did not produce any effects (Fig. S5I–J). Thus, D2R-stimulation enhanced the neuronal population's representation of numerosities in the memory delay period.

D1R Manipulation did not Modulate Working Memory Coding at Single Neuron or Population Levels

We assessed D1R manipulation on working memory coding by either stimulating or blocking D1R using SKF81297 or SCH23390, respectively. We found no differences in coding strength of sample numerosities at the single neuron level when applying the D1R agonist SKF81297 (Fig. S3A–H) or the

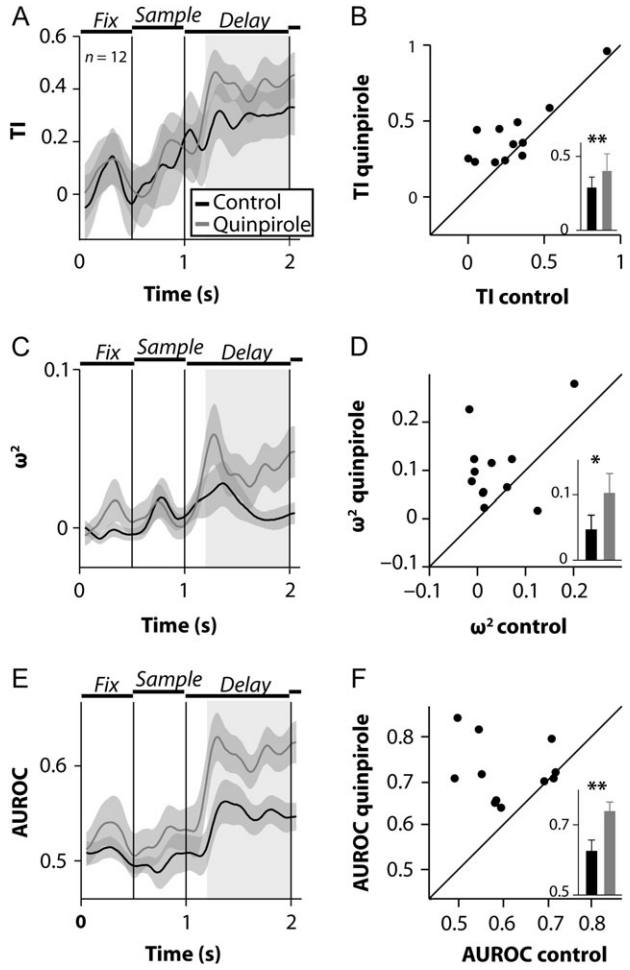

Figure 3. D2R stimulation enhanced numerosity coding during working memory at single neuron level. (*A*) Time-dependent TIs for control (*black*) and drug (*red*) conditions from fixation onset to the end of the delay 1 period for working memory-selective neurons. (*B*) TIs during the delay period for quinpirole application plotted agains TIs in control conditions; each dot corresponds to one single unit, inset shows mean over neurons. (*C*) Time course of PEV (ω^2) (layout as in (*A*)). (*D*) PEV (ω^2) during quinpirole application plotted against PEV in control conditions (layout as in (*B*)). (*E*) Time course of AUROCs (layout as in (*A*)). (*F*) AUROCs during quinpirole application plotted against AUROCs in control conditions (layout as in (*B*)). Gray windows in (*A*,*C*,*E*) denote analysis window in the delay 1 period. Error bars and colored shaded areas represent standard errors of the mean (SEMs). * $p < 0.05$, ** $p < 0.01$ (signed rank test).

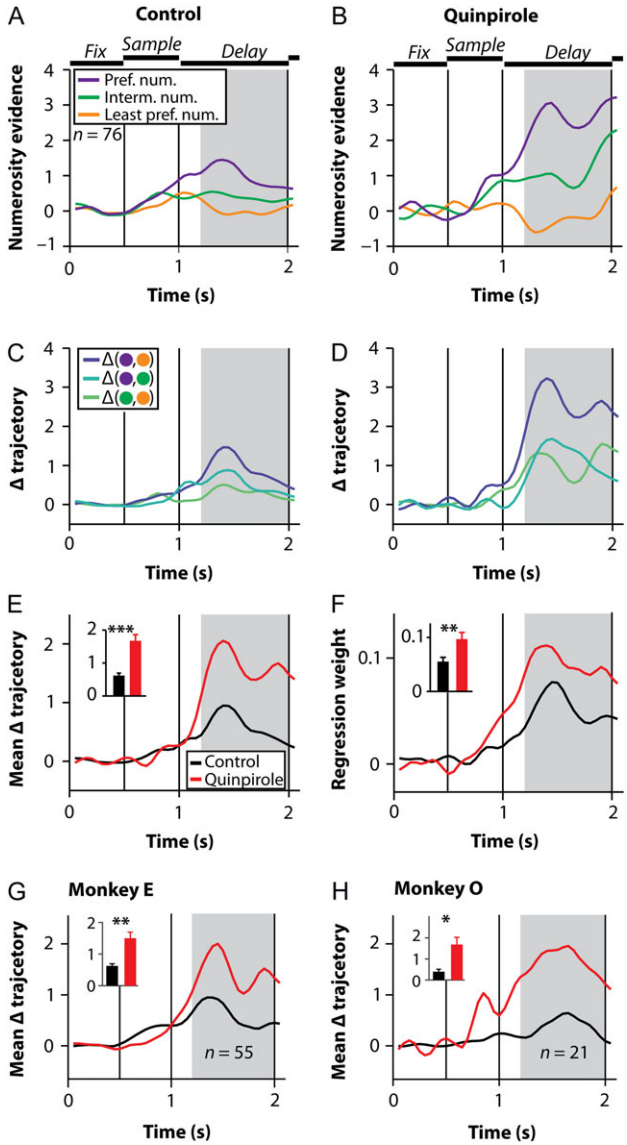

Figure 4. D2R stimulation enhanced numerosity coding during working memory at population level. (*A*) Population responses projected on the numerosity axes for control conditions. Trajectories represent the time-dependent numerosity evidence control conditions for different numerosities represented by the neuronal population. (*B*) Time-dependent numerosity evidence for the same population of neurons under quinpirole (layout as in (*A*)). (*C*) Absolute differences between all pair-wise sample trajectory combinations (see (*A*)) in control conditions. (*D*) Absolute differences between all pair-wise sample trajectory combinations under quinpirole (layout as in (*C*)). (*E*) Mean trajectory difference (i.e., mean of curves in (*C and D*)) for control conditions (*black*) and drug conditions (*red*). D2R stimulation significantly enhanced mean trajectory difference in the delay 1 period (inset). (*F*) Population average regression weights for the factor numerosity in the linear regression model for control and drug conditions (interaction term for sample and drug is either subtracted or added, respectively, see Materials and Methods). (*G*) Mean trajectory difference for monkey E (layout as in (*E*)). (*H*) Mean trajectory difference for monkey E (layout as in (*E*)). Gray shaded areas denote analysis window, error bars represent SEMs (estimated by bootstrapping). *** $p < 0.001$, ** $p < 0.01$, * $p < 0.05$ (bootstrapping in (*E*) and signed rank test in (*F*)).

D1R antagonist SCH23390 (Fig. S4A–H). In addition, we performed population analysis to assess D1R effects on working memory coding using the same linear regression analysis as described previously (Mante et al. 2013). We found no significant differences of working memory coding for neurons tested with the D1R agonist (Fig. S3I–J) or D1R antagonist (Fig. S4I–J). Thus, D1R manipulation, in contrast to D2R stimulation, did not affect memory-delay selectivity for quantities at the single neuron or population level.

Dopamine Receptors Modulated the PFC Population's Response Dynamics

To assess neuronal population's response dynamics, we analyzed population responses of all recorded 76 neurons tested for D2R-effects by representing the population single-unit activity in a low-dimensional space using PCA (see Materials and Methods), extracting shared activity patterns prominent in the population response (Harvey et al. 2012). Population activity represented by the first three principal components (PCs) showed prominent shifts in population activity after sample onset and at the beginning of the memory delay period as a

function of numerosities (Fig. 5A). After stimulating D2Rs with quinpirole, population activity followed similar trajectories, but showed improved differentiation between different numerosities (Fig. 5B). Discrimination between numerosity representations, quantified by the Euclidean distance between population trajectories for all numerosity combinations (Fig. 5C, see Materials and Methods), was increased by D2R stimulation in the delay period (Fig. 5D). The mean differences between the trajectories were significantly higher during D2R-stimulation (Fig. 5E) (change in mean Δtrajectory = +0.37 ± 0.18, p = 0.02, bootstrapping).

To evaluate population dynamics further, we quantified the speed with which the population trajectories traveled through state space by calculating the average rate of change of state space trajectories (Stokes et al. 2013) (see *Materials and Methods*). Delay-period onset (and sample onset) induced a rapid acceleration of the population trajectories (Fig. 5F). The distances traveled by the trajectories were greater after D2R stimulation (Fig. 5F, bottom inset, change in traveled distance = +2.1 ± 1.3, p = 0.04, bootstrapping). Velocity decreased during the delay period, indicating a more stable state during working memory (Fig. 5F, top inset). Thus, D2R stimulation enhanced velocity particularly during the dynamic (i.e. transition) periods of the population activity. As above, we verified PCA analysis by using shuffled data, cross-validation, and simulated data (Fig. S7). Thus, D2R stimulation increased the neuronal population's response dynamics, enhancing the trajectories' separability in state space. Interestingly, D1R stimulation (Fig. 6A,B), but not D1R blockage (Fig. 6C,D), significantly decreased the population's velocity in state space (change in velocity = –2.4 ± 1.2, p = 0.02, change in traveled distance = –2.4 ± 1.3, p = 0.004, bootstrapping, control analyses in Fig. S8). Application of saline (NaCl) did not produce any effects (Fig. S5K–L). Thus, D1Rs and D2Rs showed opposite effects on coding stability during transition stages.

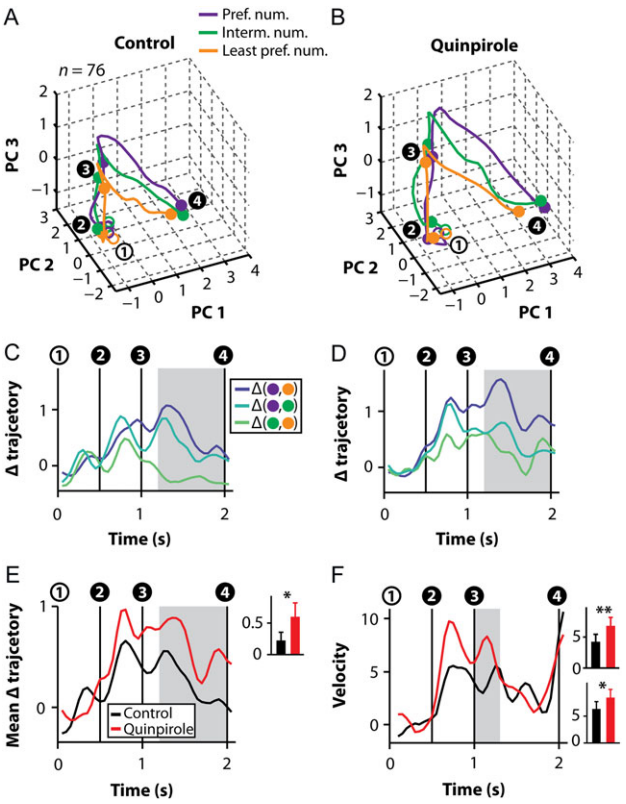

Figure 5. D2R stimulation enhanced response dynamics of prefrontal populations. (*A*) The activity of all recorded neurons (n = 76) recorded with D2R stimulation represented in state space by the first three PCs for control conditions. (*B*) Same neurons as in (*A*) represented in state space during quinpirole application (layout as in A). (*C*) Euclidean distance between all pair-wise trajectories (see (*A*)) for control conditions. (*D*) Euclidean distance between all pair-wise trajectories (see (*B*)) during quinpirole application (layout as in (*C*)). (*E*) Mean trajectory distance (i.e,. mean of curves in (*C and D*)) for control (*black*) and drug (*red*) conditions. D2R stimulation significantly increased trajectory distance in the delay 1 period (inset). (*F*) Mean trajectories' velocity, i.e. the rate of change of positions in state space over time, for control (*black*) and drug (*red*) conditions. D2R stimulation increased the population's mean velocity in state space at the beginning of the delay period after sample offset (top inset) as well as the distance traveled by the trajectories through state space (bottom inset). Numbers indicate trial events, 1: fixation onset, 2: sample onset: 3: delay 1 start, 4: delay 1 end (rule cue onset). Gray shaded areas denote analysis windows, error bars represent SEMs (estimated by bootstrapping). ** p < 0.01, * p < 0.05 (bootstrapping).

Computational Modeling Suggests Specific Mechanism for D2R Modulation

We implemented a biophysically plausible network attractor model of object working memory (Brunel and Wang 2001; Wang 2002; Goodman and Brette 2009) to investigate possible mechanisms of D2R actions. The model consisted of pyramidal cells and interneurons with recurrent excitatory and recurrent inhibitory connections (Fig. 7A). These cell types generate attractor networks with stable spontaneous activity states and stable persistent (reverberatory) activity states (Fig. 7B) modeling information held in working memory (see Materials and Methods). Connections were modeled by excitatory pyramidal-to-pyramidal and pyramidal-to-interneuron AMPA and NMDA glutamatergic synapses, as well as inhibitory interneuron-to-interneuron and interneuron-to-pyramidal GABAergic synapses.

When transiently stimulating one of three selective subsets of pyramidal cells, corresponding to neurons selective for one of

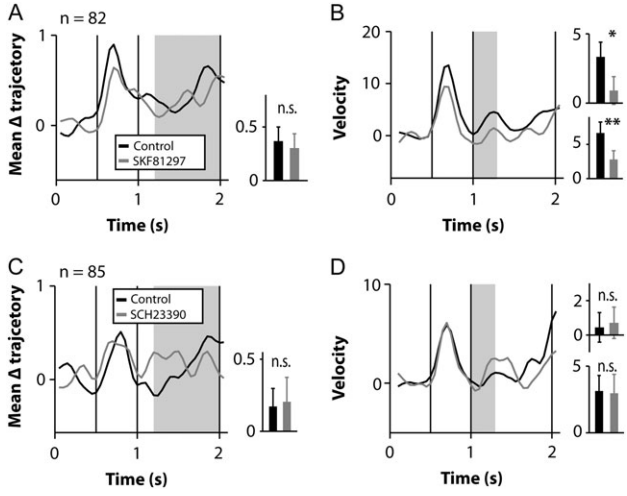

Figure 6. D1R stimulation decreased response dynamics of prefrontal populations. (*A*) PCA analysis for SKF81297. Same conventions as in Fig. 5E for D1R stimulation. (*B*) Same conventions as Fig. 5F for SKF81297. (*C*) PCA analysis for SCH23390. Same conventions as in Fig. 5E for blocking D1Rs. (*D*) Same conventions as Fig. 5F for SCH23390. Gray shaded areas denote analysis windows, error bars represent SEMs (estimated by bootstrapping). ** p < 0.01, * p < 0.05 (bootstrapping).

the three numerosities, the pyramidal cell population switched from a spontaneous activity state to a stable persistent activity state without further stimulation (Fig. 7B). In vitro studies using prefrontal slices suggest that D2R stimulation decreases responsiveness to GABA in pyramidal cells (Seamans et al. 2001; Trantham-Davidson et al. 2004). We thus studied effects of decreasing the GABA conductance in interneuron-to-pyramidal synapses, which lead to an overall increase in spiking activity that impaired the network's stable spontaneous activity state under only slight decreases of GABA conductances (Fig. 7C).

D2R stimulation has been shown to modulate interneuron excitability (Zhong and Yan 2016). We implemented this effect by increasing AMPA conductances in interneurons, leading to an increase in inhibition and to a breakdown of the network's persistent activity state (Fig. 7D). However, by combining both modulations, disinhibition of pyramidal cells by decreasing GABA conductances was balanced by increasing AMPA conductances in interneurons, i.e., increasing interneuron excitability. Both spontaneous and persistent activity states remained stable over a larger range (Fig. 7E). The network showed a small increase in spontaneous activity in addition to a prominent increase of persistent activity, increasing the neurons' selectivity to a sample stimulus during the delay memory period, reproducing our key experimental results.

Discussion

We show that stimulation of prefrontal D2Rs enhanced working memory representations of numerosities both on single neuron and on population levels. D2Rs changed the flexibility of neuronal population activity by increasing the population's response dynamics. By using a computational model of prefrontal networks, we suggest a mechanism by which D2Rs control prefrontal working memory networks.

D2R Improves Feature-based Working Memory Representations

These results provide a neuronal basis for D2R modulation of working memory in primates and complement reported behavioral effects of D2R manipulation. D2R stimulation has been shown to influence working memory performance in monkeys and humans by increasing or decreasing performance (Arnsten et al. 1995; Mehta et al. 2001; Gibbs and D'Esposito 2005; Von Huben et al. 2006), depending on the subject's baseline performance (Clark and Noudoost 2014). In addition, D2Rs play a role in mediating cognitive flexibility (Klanker et al. 2013). Blocking D2Rs impairs the ability of rats to switch between different response strategies (Floresco et al. 2006). In monkeys, blocking prefrontal D2Rs impairs learning of new association rules and reduces neural selectivity for the learned saccade direction (Puig and Miller 2015), while stimulating D2Rs increased neural selectivity for task rules in the same numerical switching task (Ott et al. 2014).

Despite this behavioral impact, a neuronal correlate of D2R modulation of working memory was lacking so far. In monkeys performing a oculomotor delayed-response (ODR) task to test spatial working memory, D2Rs did not modulate persistent delay activity (Wang et al. 2004). However, because the ODR task allows for saccadic motor preparation, many neurons might reflect response-related signals rather than pure working memory representations during the delay (Takeda and Funahashi 2004; Markowitz et al. 2015). Here, we excluded motor preparation during the delay by forcing the monkeys to

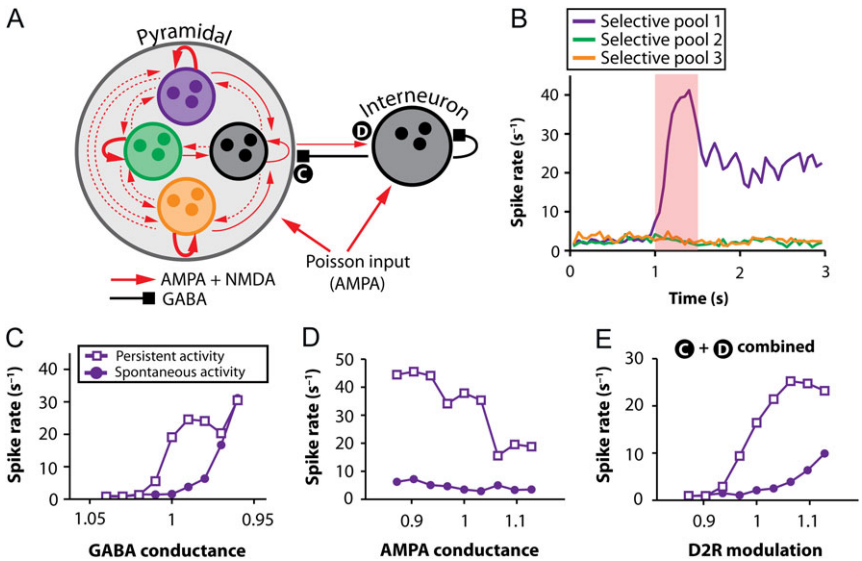

Figure 7. Attractor network model for D2R modulation of working memory. (*A*) Within the network, recurrent excitatory connections by AMPA and NMDA receptors are structured in three selective pyramidal cell groups (*colored circles*), characterized by strong recurrent connections within one selective pool w_+ (*thick arrows*) (see Materials and Methods) and weak synaptic connections w_- between pools (*dashed arrows*) and from non-selective neurons. Other connections have weight $w = 1$ (*thin arrows*). An interneuron pool is characterized by recurrent GABA connections and interneuron-to-pyramidal GABAergic connections subject to neuromodulation (*C*). Pyramidal cells project to interneurons, too (*D*). External Poisson input is mediated by AMPA receptors. For details see Materials and Methods. (*B*) Population activity before and after transient stimulation (*red shaded area*) of the first selective pool (*purple curve*), showing two distinct stable states, a spontaneous activity state before stimulation and a persistent activity state after stimulation. (*C*) Simulation under systematic variation of GABA conductances in interneuron-to-pyramidal synapses. Plotted is the spontaneous activity (*closed circles*) before stimulation and the persistent activity after stimulation (*open squares*) of the stimulated selective pool (*purple*), corresponding to a bifurcation diagram (Brunel and Wang 2001). Note that a decrease in GABA conductance is plotted to the right, since D2R stimulation has been shown to decrease GABA transmission. (*D*) Same conventions as in (*C*) with systematic variation of AMPA conductances from pyramidal cells to interneurons. (*E*) Proposed D2R modulation combing both GABA modulation in (*C*) and AMPA modulation in (*D*).

make a response-independent and rule-cued decision. Persistent activity in the delay phase thus reflects feature-based working memory representations devoid of motor preparation. In this situation, we find that D2R stimulation robustly enhanced persistent mnemonic activity in PFC neurons, thus resolving the discrepancy between behavioral and neuronal effects. It is also conceivable that feature-based working memory and spatial working memory are distinctly represented by PFC neurons and differentially modulated by dopamine (Wilson et al. 1993). We recorded neurons in the vicinity of the principal sulcus of both monkeys. Recording sites overlapped with a previous study, which did not find D2R modulation of delay period activity (Wang et al. 2004), although our recordings extended more ventrally of the principal sulcus, which is possibly more strongly involved in feature-based working memory (Wilson et al. 1993). Although anatomical differences might contribute to the distinct results, the largely overlapping recording sites together with studies emphasizing that visual features and spatial locations are represented in both ventral and dorsal lateral PFC (Rao et al. 1997) make this possibility unlikely.

In contrast to the clear D2R effects, D1R manipulation did not seem to modulate persistent working memory activity in the current study. This was unexpected, given that several studies reported D1R modulation of spatial working memory signals (Williams and Goldman-Rakic 1995; Vijayraghavan et al. 2007). While D1R stimulation decreased neuronal firing rates (Ott et al. 2014), D1R effects were not restricted to unspecific changes in firing rates. D1R activation increased the persistent rule-related signals in the same task using the same drug amount as in the present study (Ott et al. 2014). A possible explanation for this discrepancy might be related to the prominent dose-dependency of D1R effects. Reported D1R manipulations followed an inverted-U function and produced varying effects, including an improvement of spatial workings memory signals by both stimulating and blocking D1Rs (Williams and Goldman-Rakic 1995; Vijayraghavan et al. 2007). Thus, effects observed after D1R manipulation seem to heavily depend on the baseline activation of D1Rs. This D1R response function might account for the differences between our and other studies. Alternatively, or in addition, D1R modulation might differentially modulate spatial (Williams and Goldman-Rakic 1995; Vijayraghavan et al. 2007) and feature-based (our study) working memory. Further studies directly comparing dopamine receptor modulation of spatial and feature-based working memory representations might reveal if D1Rs or D2Rs differentially modulate both signals.

Putative D2R Mechanism Involves Differential Modulation of Interneurons and Pyramidal Cells

We implemented a biophysically plausible spiking neural network in which synaptic connections are described on a single neuron level. By simulating recurrent excitatory and inhibitory connections, the activity of neurons in the network show characteristic stable attractor states. This approach was used previously to describe working memory and decision-making processes (Durstewitz et al. 2000a; Wang 2002; Constantinidis and Wang 2004). Using this model, we investigated possible D2R mechanisms of action by incorporating D2R modulation of synaptic conductances. We constrained possible synaptic modulation by investigating putative D2R targets supported by in vitro studies (Seamans et al. 2001; Trantham-Davidson et al. 2004; Zhong and Yan 2016), although we acknowledge diverse D2R effects found in vitro (Seamans and Yang 2004). Our modeling results suggest that D2Rs act on synaptic transmission to modulate working memory representations via two distinct mechanisms. First, we propose that D2Rs change interneuron-to-pyramidal signaling by reducing inhibitory postsynaptic currents (IPSCs) mediated by GABA receptors in pyramidal cells (Seamans et al. 2001), thus disinhibiting pyramidal cell firing. Second, D2R stimulation might increase AMPA synaptic currents in interneurons (Zhong and Yan 2016), thereby increasing interneuron excitability and possibly balancing excessive excitatory effects induced by D2R stimulation. Combined, the proposed D2R mechanism accounts for two key experimental results of the current study. First, D2R stimulation increased neuronal activity of prefrontal neurons (Ott et al. 2014), which has also been reported by previous studies (Wang and Goldman-Rakic 2004; Wang et al. 2004). Second, D2R activation increased the differentiation between persistent activity and spontaneous activity in the network model, thus enhancing working memory selectivity.

The proposed mechanism assumes that D2Rs influence interneurons and pyramidal cells differentially. This assumption is supported by studies that showed a differential impact of dopamine on pyramidal cells and interneurons (Gao and Goldman-Rakic 2003). Dopamine inhibits putative interneurons, whereas it both excites and inhibits putative pyramidal cells (Jacob et al. 2013). Thus, differential modulation of cortical cell types might be a key mechanism by which dopamine controls cortical networks. In agreement with previous reports, our findings support a strong role of interneurons in maintaining working memory representations (Rao et al. 2000; Constantinidis et al. 2002). D2Rs are abundantly expressed in PFC interneurons, particularly in parvalbumin-positive interneurons (de Almeida and Mengod 2010), which have been shown to modulate response gain in rodent cortex (Wilson et al. 2012). Thus, D2R modulation of interneuron signaling might mediate the observed changes in working memory activity. The neural network model provides hypotheses about micro-circuit mechanisms that can now be tested empirically (Wang et al. 2013). Specifically, we hypothesize that experimentally manipulating GABA currents in prefrontal networks might modulate the persistent activity of neurons similarly as observed in the model.

Our results complement studies investigating possible mechanisms of D1Rs (Durstewitz and Seamans 2008). It has been proposed that D1Rs modulate the network's persistent activity by changing recurrent NMDA conductances (Durstewitz et al. 2000b; Brunel and Wang 2001), which increases persistent delay activity of single neurons in the model. This result reproduces experimental studies reporting an enhancement of selective response in the delay period of single neurons after D1R stimulation (Vijayraghavan et al. 2007; Ott et al. 2014). Thus, D2Rs and D1Rs might act on prefrontal networks by distinct physiological mechanisms (Ott et al. 2014).

Dopamine Receptors Modulate Population Dynamics

Because neuronal responses show high complexity and variability at the single neuron level (Rigotti et al. 2013), we explored whether computations in PFC might emerge from the dynamics of populations of neurons (Mante et al. 2013). We described neuronal responses in the framework of dynamical systems in which the activity of neuronal population can be described as a dynamical process revealing shared activity patterns that are prominent in the population response (Cunningham and Yu 2014). This allowed us to study dopamine

receptor modulation of PFC population properties. D2R activation increased working memory representations of numerosities at the population level independently of general shifts in neuronal activity, suggesting that D2Rs interact with mechanisms generating persistent working memory activity. This working memory representation can be realized through sequence-based circuit dynamics not captured by single neuron analyses but by our state space analysis (Harvey et al. 2012). State space analysis revealed how neuromodulation can change the dynamic properties of neuronal populations. D2R stimulation increased the state space distance between trajectories during working memory. As a consequence, the neuronal system can differentiate more reliably between working memory representations of numerosities.

At the onset of visual stimulation with numerosities as well as during the transition from visual to mnemonic processing during the delay, population responses were characterized by high dynamic phases. These instances of high population dynamics were followed by a more stable phase during working memory. This characteristic response dynamic was similarly observed during flexible decision-making (Stokes et al. 2013). D2R stimulation enhanced the dynamic responses of PFC populations, thereby enhancing state flexibility in PFC populations. In contrast, D1R stimulation decreased population dynamics, thereby maintaining PFC populations in a more stable state.

These results support computational models which suggest that dopaminergic modulation of prefrontal working memory networks balance stability and flexibility of working memory representations (Seamans et al. 2001; Seamans and Yang 2004; Durstewitz and Seamans 2008; Rolls et al. 2008). According to this hypothesis, a D1R-dominated state stabilizes prefrontal representations, whereas a D2R-dominated state destabilizes them enabling switching between different representations thus mediating flexibility. Our results provide experimental evidence that D2Rs contribute to controlling stability and flexibility of prefrontal working memory representations. These results contribute to the idea that excessive cortical D2R activation contributes to psychosis by destabilizing working memory representations in schizophrenic patients (Winterer and Weinberger 2004; Rolls et al. 2008). Thus, excessive D2R activation might attribute aberrant salience to external events or internal representations, leading to symptoms of psychosis such as sensory hallucinations and intrusions of thought (Kapur 2003). In conclusion, prefrontal dopamine receptors might mediate dynamic cognitive control (Cools 2015) by balancing the stability of persistent activity during working memory with the flexibility of prefrontal networks needed for adaptive, goal-directed behavior.

Supplementary Material

Supplementary material can be found at: http://www.cercor.oxfordjournals.org/

Author Contributions

T.O. designed and performed experiments, analyzed data and wrote the paper. A.N. designed experiments and wrote the paper.

Funding

Grants from the German Research Foundation (DFG) to A.N. (NI 618/5-1).

Notes

Conflict of Interest: None declared.

References

Andersen PH, Jansen JA. 1990. Dopamine receptor agonists: selectivity and dopamine D1 receptor efficacy. Eur J Pharmacol Mol Pharmacol. 188:335–347.

Arnsten AFT, Cai JX, Steere JC, Goldman-Rakic PS. 1995. Dopamine D2 receptor mechanisms contribute to age-related cognitive decline: the effects of quinpirole on memory and motor performance in monkeys. J Neurosci. 15: 3429–3439.

Baddeley A. 2012. Working memory: theories, models, and controversies. Annu Rev Psychol. 63:1–29.

Bongard S, Nieder A. 2010. Basic mathematical rules are encoded by primate prefrontal cortex neurons. Proc Natl Acad Sci USA. 107:2277–2282.

Brunel N, Wang XJ. 2001. Effects of neuromodulation in a cortical network model of object working memory dominated by recurrent inhibition. J Comput Neurosci. 11:63–85.

Clark KL, Noudoost B. 2014. The role of prefrontal catecholamines in attention and working memory. Front Neural Circuits. 8:1–19.

Constantinidis C, Wang X-J. 2004. A neural circuit basis for spatial working memory. Neurosci. 10:553–565.

Constantinidis C, Williams G V, Goldman-Rakic PS. 2002. A role for inhibition in shaping the temporal flow of information in prefrontal cortex. Nat Neurosci. 5:175–180.

Cools R. 2015. The cost of dopamine for dynamic cognitive control. Curr Opin Behav Sci. 4:1–8.

Cunningham JP, Yu BM. 2014. Dimensionality reduction for large-scale neural recordings. Nat Neurosci. 17:1500–1509.

de Almeida J, Mengod G. 2010. D2 and D4 dopamine receptor mRNA distribution in pyramidal neurons and GABAergic subpopulations in monkey prefrontal cortex: implications for schizophrenia treatment. Neuroscience. 170:1133–1139.

Durstewitz D, Seamans JK. 2008. The dual-state theory of prefrontal cortex dopamine function with relevance to catechol-o-methyltransferase genotypes and schizophrenia. Biol Psychiatry. 64:739–749.

Durstewitz D, Seamans JK, Sejnowski TJ. 2000a. Neurocomputational models of working memory. Nat Neurosci. 3 (Suppl): 1184–1191.

Durstewitz D, Seamans JK, Sejnowski TJ. 2000b. Dopamine-mediated stabilization of delay-period activity in a network model of prefrontal cortex. J Neurophysiol. 83:1733–1750.

Eiselt A-K, Nieder A. 2013. Representation of abstract quantitative rules applied to spatial and numerical magnitudes in primate prefrontal cortex. J Neurosci. 33:7526–7534.

Floresco SB, Magyar O. 2006. Mesocortical dopamine modulation of executive functions: beyond working memory. Psychopharmacol. 188:567–585.

Floresco SB, Magyar O, Ghods-Sharifi S, Vexelman C, Tse MTL. 2006. Multiple dopamine receptor subtypes in the medial prefrontal cortex of the rat regulate set-shifting. Neuropsychopharmacology. 31:297–309.

Fuster J. 2008.The prefrontal cortex. 4th ed. London: Academic Press.

Gao W-J, Goldman-Rakic PS. 2003. Selective modulation of excitatory and inhibitory microcircuits by dopamine. Proc Natl Acad Sci USA. 100:2836–2841.

Gibbs SEB, D'Esposito M. 2005. Individual capacity differences predict working memory performance and prefrontal activity following dopamine receptor stimulation. Cogn Affect Behav Neurosci. 5:212–221.

Goodman DFM, Brette R. 2009. The brian simulator. Front Neurosci. 3:192–197.

Harvey CD, Coen P, Tank DW. 2012. Choice-specific sequences in parietal cortex during a virtual-navigation decision task. Nature. 484:62–68.

Hyttel J. 1983. SCH 23390 – the first selective dopamine D-1 antagonist. Eur J Pharmacol. 91:153–154.

Jacob SN, Nieder A. 2014. Complementary roles for primate frontal and parietal cortex in guarding working memory from distractor stimuli. Neuron. 83:226–237.

Jacob SN, Ott T, Nieder A. 2013. Dopamine regulates two classes of primate prefrontal neurons that represent sensory signals. J Neurosci. 33:13724–13734.

Kapur S. 2003. Psychosis as a state of aberrant salience: a framework linking biology, phenomenology, and pharmacology in schizophrenia. Am J Psychiatry. 160:13–23.

Klanker M, Feenstra M, Denys D. 2013. Dopaminergic control of cognitive flexibility in humans and animals. Front Neurosci. 7:1–24.

Levant B, Grigoriadis DE, DeSouza EB. 1992. Characterization of [3H] quinpirole binding to D2-like dopamine receptors in rat brain. J Pharmacol Exp Ther. 262:929–935.

Mante V, Sussillo D, Shenoy K V, Newsome WT. 2013. Context-dependent computation by recurrent dynamics in prefrontal cortex. Nature. 503:78–84.

Markowitz DA, Curtis CE, Pesaran B. 2015. Multiple component networks support working memory in prefrontal cortex. Proc Natl Acad Sci. 112:11084–11089.

Mehta MA, Swainson R, Ogilvie AD, Sahakian B, Robbins TW. 2001. Improved short-term spatial memory but impaired reversal learning following the dopamine D2 agonist bromocriptine in human volunteers. Psychopharmacol. 159:10–20.

Müller U, von Cramon DY, Pollmann S. 1998. D1- versus D2-receptor modulation of visuospatial working memory in humans. J Neurosci. 18:2720–2728.

Nieder A. 2016. The neuronal code for number. Nat Rev Neurosci. 17:366–382.

Nieder A, Freedman DJ, Miller EK. 2002. Representation of the quantity of visual items in the primate prefrontal cortex. Science. 297:1708–1711.

Nieder A, Miller EK. 2003. Coding of cognitive magnitude: compressed scaling of numerical information in the primate prefrontal cortex. Neuron. 37:149–157.

Noudoost B, Moore T. 2011. Control of visual cortical signals by prefrontal dopamine. Nature. 474:372–375.

Ott T, Jacob SN, Nieder A. 2014. Dopamine receptors differentially enhance rule coding in primate prefrontal cortex neurons. Neuron. 84:1317–1328.

Petrides M. 2005. Lateral prefrontal cortex: architectonic and functional organization. Philos Trans R Soc B Biol Sci. 360:781–795.

Puig MV, Miller EK. 2012. The role of prefrontal dopamine D1 receptors in the neural mechanisms of associative learning. Neuron. 74:874–886.

Puig MV, Miller EK. 2015. Neural substrates of dopamine D2 receptor modulated executive functions in the monkey prefrontal cortex. Cereb Cortex. 25:2980–2987.

Rao SC, Rainer G, Miller EK. 1997. Integration of what and where in the primate prefrontal cortex. Science. 276:821–824.

Rao SG, Williams G V, Goldman-Rakic PS. 2000. Destruction and creation of spatial tuning by disinhibition: GABA(A) blockade of prefrontal cortical neurons engaged by working memory. J Neurosci. 20:485–494.

Rigotti M, Barak O, Warden MR, Wang X-J, Daw ND, Miller EK, Fusi S. 2013. The importance of mixed selectivity in complex cognitive tasks. Nature. 497:585–590.

Robbins TW, Arnsten AFT. 2009. The neuropsychopharmacology of fronto-executive function: monoaminergic modulation. Annu Rev Neurosci. 32:267–287.

Rolls ET, Loh M, Deco G, Winterer G. 2008. Computational models of schizophrenia and dopamine modulation in the prefrontal cortex. Nat Rev Neurosci. 9:696–709.

Sawaguchi T, Goldman-Rakic PS. 1991. D1 dopamine receptors in prefrontal cortex: involvement in working memory. Science. 251:947–950.

Seamans JK, Gorelova N, Durstewitz D, Yang CR. 2001. Bidirectional dopamine modulation of GABAergic inhibition in prefrontal cortical pyramidal neurons. J Neurosci. 21: 3628–3638.

Seamans JK, Yang CR. 2004. The principal features and mechanisms of dopamine modulation in the prefrontal cortex. Prog Neurobiol. 74:1–58.

Seeman P, Van Tol HHM. 1994. Dopamine receptor pharmacology. Trends Pharmacol Sci. 15:264–270.

Stelzel C, Fiebach CJ, Cools R, Tafazoli S, D'Esposito M. 2013. Dissociable fronto-striatal effects of dopamine D2 receptor stimulation on cognitive versus motor flexibility. Cortex. 49:2799–2811.

Stokes MG, Kusunoki M, Sigala N, Nili H, Gaffan D, Duncan J. 2013. Dynamic coding for cognitive control in prefrontal cortex. Neuron. 78:364–375.

Takeda K, Funahashi S. 2004. Population vector analysis of primate prefrontal activity during spatial working memory. Cereb Cortex. 14:1328–1339.

Thiele A, Delicato LS, Roberts MJ, Gieselmann MA. 2006. A novel electrode-pipette design for simultaneous recording of extracellular spikes and iontophoretic drug application in awake behaving monkeys. J Neurosci Methods. 158:207–211.

Trantham-Davidson H, Neely LC, Lavin A, Seamans JK. 2004. Mechanisms underlying differential D1 versus D2 dopamine receptor regulation of inhibition in prefrontal cortex. J Neurosci. 24:10652–10659.

Vallentin D, Bongard S, Nieder A. 2012. Numerical rule coding in the prefrontal, premotor, and posterior parietal cortices of macaques. J Neurosci. 32:6621–6630.

Vijayraghavan S, Wang M, Birnbaum SG, Williams G V, Arnsten AFT. 2007. Inverted-U dopamine D1 receptor actions on prefrontal neurons engaged in working memory. Nat Neurosci. 10:376–384.

Viswanathan P, Nieder A. 2013. Neuronal correlates of a visual "sense of number" in primate parietal and prefrontal cortices. Proc Natl Acad Sci USA. 110:11187–11192.

Von HubenSN, DavisS a., LayCCKatnerSN, CreanRD, TaffeMA. 2006. Differential contributions of dopaminergic D1- and D2-like receptors to cognitive function in rhesus monkeys. Psychopharmacology. 188:586–596

Wang M, Vijayraghavan S, Goldman-Rakic PS. 2004. Selective D2 receptor actions on the functional circuitry of working memory. Science. 303:853–856.

Wang M, Yang Y, Wang C-J, Gamo NJ, Jin LE, Mazer JA, Morrison JH, Wang X-J, Arnsten AFT. 2013. NMDA receptors subserve persistent neuronal firing during working memory in dorsolateral prefrontal cortex. Neuron. 77:736–749.

Wang X-J. 2002. Probabilistic decision making by slow reverberation in cortical circuits. Neuron. 36:955–968.

Wang Y, Goldman-Rakic PS. 2004. D2 receptor regulation of synaptic burst firing in prefrontal cortical pyramidal neurons. Proc Natl Acad Sci USA. 101:5093–5098.

Williams G V, Goldman-Rakic PS. 1995. Modulation of memory fields by dopamine D1 receptors in prefrontal cortex. Nature. 376:572–575.

Wilson F a, Scalaidhe SP, Goldman-Rakic PS. 1993. Dissociation of object and spatial processing domains in primate prefrontal cortex. Science. 260:1955–1958.

Wilson NR, Runyan CA, Wang FL, Sur M. 2012. Division and subtraction by distinct cortical inhibitory networks in vivo. Nature. 488:343–348.

Winterer G, Weinberger DR. 2004. Genes, dopamine and cortical signal-to-noise ratio in schizophrenia. Trends Neurosci. 27:683–690.

Zhong P, Yan Z. 2016. Distinct physiological effects of dopamine D4 receptors on prefrontal cortical pyramidal neurons and fast-spiking interneurons. Cereb Cortex. 26:180–191.